Optimal Design and Analysis of a Novel Reluctance Axial Flux Magnetic Gear

S.A. Afsari*
Faculty of Electrical and Computer Engineering, University of Kashan, Kashan, Iran
(P.O. Box: 87317-53153)
(Phone: +983155913480 Mobile: +989126088678)
afsari@kashanu.ac.ir

Abstract: This paper proposes modelling and optimization of a new reluctance axial flux magnetic gear (RAMG) with stationary outer rotor and advantages of lower permanent magnet usage. Due to the less use of the PMs, this structure has a higher economic interest, more reliability, and very simple and robust structure than its conventional ones. Gear ratio and operating principles are extracted and verificated using 3-D finite element method (FEM) simulations. Finally, a parametric optimization is done based on effective dimensions in design procedure with maximum torque density objective function. The magnetic flux distributions of optimized RAMG are calculated by 3-D FEM, as well as static and dynamic magnetic torques are derived correspondingly.
Keywords: *reluctance magnetic gear, 3-D FEM, axial flux, torque density, flux density.*

1. Introduction

In low-speed industrial applications, an electrical machine with a mechanical gearbox is applied to save the total volume of the system by extracting the desired torque based on the performance of the mechanical gear. The most common types of mechanical gear is the spur gear, the worm gear, the rack pinion gear, the bevel gear, and the planetary gear. The torque density and the gear ratio are used to evaluate the performance of the mechanical gears. In addition to the advantages of mechanical gearbox, some problems such as: the need for lubrication, no overload protection, fracture and corrosion, noise, vibration and mechanical losses, have led to tendencies towards new systems named magnetic gears (MGs). Many initial MG technologies inspired by mechanical counterparts. Armstrong [1] and Faus [2] introduce MGs according to a mechanical spur gear. Tsurumoto and Kikuchi presented a worm based [3] and spiral based MG topology [4]. A problem with these initial MG designs was that only one to some magnets transferred torque at any given moment and this leads to a lower torque transfer. Today's advanced MGs in its general form benefit from two rotors of high-energy permanent magnets (PMs) and a middle ferromagnetic pole pieces rotor named modulators [5, 6]. Magnetic flux produced by PMs modulated by ferromagnetic pole pieces to establish an effective harmonic component with different rotational speed to rotate opposite rotor as a gear [4, 7, 8]. This topology offers some advantages such as no contact, no wear and corrosion, no noise, no need for lubrication, and as well as inherent overload protection [9, 10]. Novel MGs structure can compete with traditional mechanical types. In the last decade, various structures have been introduced to increase torque density [11, 12], minimize cogging torque [13, 14], and reduce total cost [15, 16].

In [17], a general review of magnetic gears is presented, including a discussion of the most common and upcoming topologies and a description of the working principle. A comparison of different topologies is carried out, in terms of gear ratio and torque density. [18] presents a time-saving methodology for the design and sizing of the radial MG sets. A novel high temperature superconducting bulks coaxial MG with an eccentric pole of inner rotor and Halbach arrays of outer rotor is proposed in [19] to improve the high torque density of MG. [20] presents a novel design of rotor topology for a superconductive radial flux magnetic gear to achieve sinusoidal air-gap flux density and lower cogging torque. The method is based on optimization of buried magnet's pole shape in a radial flux structure, modified by using pulse width modulation technique and variable air gap length applying the supershape formula on the iron core of the inner rotor. [21] investigates the torque performances of magnetic gear with different configurations of the modulating ring that are characterized by the shape of modulator, the position of interconnecting bridge, and the ratio of pole arc to pole pitch. The torque density characteristics for an axial flux magnetic gear using a flux-focusing topology is experimentally studied in [22]. A geometric parameter sweep analysis was utilized in order to maximize both the calculated volumetric and mass torque density. Many commercially available mechanical gears can operate with torque densities above 250 Nm/L, while for MG, the torque density is lower than 200Nm/L [23]. This means that further improvements in the MG technology is still required.

Among the different structures of radial flux (coaxial) [24], linear [25], transverse flux [26], arcuate [27], and axial flux, the axial flux (AFMG) structure has been more widely considered [28-30]. This is due to the isolation of the input and output shafts, providing the possibility of oscillation of the axes relative to each other, and lower occupation of the axial space.

The magnets used in AFMGs can be in form of surface mounted or interior [31, 32]. The magnets in high speed rotor are exposed to the impact of centrifugal force and scratch. In addition, the high cost ratio of PMs in total cost of MGs is one of the fundamental challenges of conventional MGs [15, 16]. In this paper, a novel reluctance AFMG (RAMG) structure is introduced (based on the concepts of reluctance machines) by removing PMs in high-speed rotor. PMs elimination in high speed rotor, reduces the core loss and result in higher efficiency. The other PM rotor will keep stationary and gear ratio will be obtain through the high speed reluctance rotor and the middle low speed modulator rotor. Fig 1, shows the exploded conceptual structure of a

conventional and RAMG. In [33] a radial flux reluctance MG is introduced and compared with traditional coaxial MG in gear ratio and torque transmission. A similar structure of reluctance MG is introduced in [34] using superconducting material in inner and outer rotor of coaxial structure with a single middle PM rotor to achieve a higher torque density in exchange of more cost. [35] presents a coaxial MG with reluctance outer rotor and stationary inner PM rotor. Parametric analysis and torque performance results are extracted using 2-D finite element method (FEM) analysis.

2. Operation principle of RAMGs

Sections of different rotor are shown in Fig. 2. According to the general parameters in Fig. 2 and computing magneto motive force (MMF) distribution and reluctance distribution of different rotors, magnetic field distribution and gear ratio of the RAMG can be extracted. In Fig. 2, the magnetic field is arising from stationary PM rotor and provides desired MMF. Based on the PM's pole pitch, the distribution of MMF can be expressed in terms of Equation 1:

$$F_s = F_{s1}\cos(n_m\alpha) \tag{1}$$

where F_{s1} is the amplitude of MMF, n_m is the pole pairs of the stationary rotor, and α is the mechanical angle.

By rotating middle modulator rotor, the reluctance of the magnetic path will change. According to the structure of modulator low speed rotor, the permeance distribution can be expressed in terms of Equation 2:

$$\Lambda_m = \lambda_{m0} + \lambda_{m1}\cos(p_s\alpha - p_s\omega_r t + p_s\alpha_{m0}) \tag{2}$$

where, λ_{m0} and λ_{m1} are mean and amplitude of modulator permeance, respectively. p_s, ω_r and α_{m0} are the number of modulators, angular speed and initial angle of low speed modulator rotor, respectively.

The high speed rotor will be rotated by the reluctance changing. Similarly, the distribution of the permeance of this rotor can also be expressed by Equation 3:

$$\Lambda_r = \lambda_{r0} + \lambda_{r1}\cos(n_r\alpha - n_r\omega_m t + n_r\alpha_{r0}) \tag{3}$$

where, λ_{r0} and λ_{r1} are mean and amplitude of high speed permeance, respectively. n_r, ω_m, α_{r0} are the number of reluctance teeth, angular speed, and initial angle of high speed rotor, respectively.

Magnetic flux, produces by the magnets and passes from variable reluctance space of the middle rotor and reluctance rotor, can be expressed as Equation 4:

$$\begin{aligned}
&\phi(\alpha,t)\\
&= F_s\,\Lambda_m\,\Lambda_r\\
&= F_{s1}\lambda_{m0}\lambda_{r0}\cos(n_m\alpha)\\
&\quad + 0.5F_{s1}\lambda_{m0}\lambda_{r1}\left[\cos((n_r+n_m)\alpha - n_r\omega_m t + n_r\alpha_{r0}) + \cos((n_r-n_m)\alpha - n_r\omega_m t + n_r\alpha_{r0})\right]\\
&\quad + 0.5F_{s1}\lambda_{m1}\lambda_{r0}\left[\cos((p_s+n_m)\alpha - p_s\omega_r t + P_s\alpha_{m0}) + \cos((p_s-n_m)\alpha - p_s\omega_r t + P_s\alpha_{m0})\right]\\
&\quad + 0.25F_{s1}\lambda_{m1}\lambda_{r1}\left[\cos((p_s+n_r+n_m)\alpha - (p_s\omega_r + n_r\omega_m)t + (p_s\alpha_{m0} + n_r\alpha_{r0}))\right.\\
&\qquad + \cos((p_s-n_r+n_m)\alpha - (p_s\omega_r - n_r\omega_m)t + (p_s\alpha_{m0} - n_r\alpha_{r0}))\\
&\qquad + \underline{\cos((p_s+n_r-n_m)\alpha - (p_s\omega_r + n_r\omega_m)t + (p_s\alpha_{m0} + n_r\alpha_{r0}))}\\
&\qquad \left. + \underline{\cos((p_s-n_r-n_m)\alpha - (p_s\omega_r - n_r\omega_m)t + (p_s\alpha_{m0} - n_r\alpha_{r0}))}\right]
\end{aligned} \tag{4}$$

Based on the above-mentioned relationship, the main harmonics can be determined in order to create the effective gear ratio and torque transmission. The 8th and 9th sentences of Equation 4 are the magnetic flux components modulated by modulators. The condition of pole pairs to obtain the gear ratio between the high speed rotor and the low speed rotor which can rotate the output rotor in a different speed than the input rotor is true in these sentences ($n_m \neq 0,\ n_m = p_s \pm n_r \pm n_m$). Hence, the angular speed of magnetic flux density will be equal to: $p_s\omega_r \pm n_r\omega_m$. Due to the lack of permanent magnets in the high speed and low speed rotors, the angular speed of magnetic flux density in the high speed rotor and low speed rotor are zero. Hence gear ratio can be calculated by Equation 5:

$$0 = p_s\omega_r \pm n_r\omega_m \Rightarrow G_r = \frac{\omega_m}{\omega_r} = \mp\frac{p_s}{n_r} \tag{5}$$

Thus, it can be concluded that the relation between the number of poles, modulators and reluctance teeth must be equal to Equation 6:

$$2n_m = P_s \pm n_r \tag{6}$$

The positive or negative sign will be selected, according to the coupled harmonic. Due to the high harmonic number and variation in magnetic flux, it is expected that the transmitted torque have high fluctuations.

3. Modelling and parametric optimization of RAMG

In order to optimal design of RAMG in finite element software, the various dimensions of the gear are optimized according to Figs. 2 and 3. The purpose of optimization is to maximize the torque density transmission in this structure and taking into account the design constraints.

3-D FEM simulation predicts the best results in terms of mesh balancing reliability, speed, quality, size, and design characteristics. Flux density distribution and static torque calculations are performed by steady 3-D FEM simulations while cogging torque calculations are performed by transient 3-D FEM. The nonlinear discretised governing equations that model MG performance are solved at each time step using a Newton-Raphson iteration (tolerance 10^{-3}, relaxation factor 0.15) with a

Multifrontal Massively Parallel Sparse Direct Solver (MUMPS) for the linear sub-system at each iteration (precision for scaling 10^{-3}). To produce the optimal mesh, an adaptive mesh refinement is performed in critical regions using an iterative procedure. The mesh is refined (20 times leading to reduction in energy error from 37.8% in first pass to 0.0312% in last pass) in areas of highest error density. When changes in selected parameters (percentage of energy error) are less than 0.1%, the mesh refinement terminates. The optimization takes about 57 hour by a core i7-8700 6-core processor and 64GB RAM. All simulations are done around pull out torque (maximum static torque) point.

Optimization results of different parameters are shown in Table 1, based on maximum torque density objective function. These results are derived using 3-D FEM modelling and constraints considered in Table 1. In this process, the inner and outer radius, air gaps, number of poles, and gear ratio are considered constant.

According to Table 1, the gear ratio will be +1:5. Increasing the thickness of the PMs, increases the MMF, and on the other hand, increases the reluctance of magnetic path, so the optimal thickness is obtained *9mm* according to Table 1. The reluctance of teeth and modulators thickness not only effects on total reluctance but also can cause leakage flux and weak magnetic coupling. So the optimum length of *11mm* and *8mm* is obtained for teeth and modulators, respectively. Core length depends on saturation level of core due to the flux density of PMs. According to the results of the optimization, output performances of RAMG can be extracted. The paths of magnetic potential lines and magnetic field path in different regions of optimal RAMG are shown in Fig. 4.

Axial component of magnetic field distribution in middle height and radius of high and low speed air gaps are shown in Fig. 5. Proximity to the source of MMF in high speed air gap, increases the amplitude of this component. As can be seen in Fig. 6, the amplitude of magnetic field distribution in different regions show some hot spots of about *2.3 T* in sharp points in some moments.

According to the above structure and dimensions of RAMG, the static and dynamic torque in high and low speed rotors can be calculated by 3-D FEM analysis as Figs. 7 and 8, respectively. In static analysis, the reluctance rotor rotated about 90 mechanical degree and two other rotors are kept stationary. Calculated static torque is equal to 1.5 Nm and 7.5 Nm for high speed and low speed rotors, respectively. Maximum static torque occurs in initial zero mechanical degree. Thus, the initial mechanical angle for dynamic simulations will be set in maximum point of static torque, named pull out torque. In dynamic simulation, the high speed reluctance rotor and low speed modulator rotors are rotated in same directions according to the gear ratio. So the average torque of about 1.5Nm and 7.5Nm and cogging torque of about 4.3Nm and 1.7Nm for high speed and low speed rotors can be obtain, respectively. As can be seen, the dynamic torque has a considerable pulsation and cogging torque. That's because the gear ratio is an integer number, so all the teeth meets the edge of modulators and PMs at the same times and reluctance changes directly effects on torque transmission. Results of optimal RAMG and initial RAMG are presented in Table 2.

4. Conclusion

In this paper a novel RAMG is introduced. This model exhibits superior advantages than the conventional axial flux MGs, especially in reducing PMs consuming and ease of construction. The same treatment of analytical analysis and 3-D FEM in gear ratio shows the high precision of proposed model. The 3-D FEM was applied to investigate the effects of different rotor dimensions on the torque density. It has been concluded that the optimal dimensions of RAMG lead to torque density of about 11.07 kNm/m^3.

5. References

[1] Armstrong C. G., "Power transmitting device", USA Patent 687,292, (1901).

[2] Faus H. T., "Magnet gearing", USA Patent 2,243,555, (1941).

[3] Kikuchi S. and Tsurumoto K., "Design and characteristics of a new magnetic work gear using permanent magnet", *IEEE Trans. Mag.*, **29**(6), pp. 2923-2925 (1993).

[4] Tsurumoto K. and Kikuchi S., "A new magnetic gear using permanent magnet", *IEEE Transactions on Magnetics*, **23**(5), pp. 3622- 3624 (1987).

[5] Atallah K., Howe D., "A novel high-performance magnetic gear", *IEEE Trans. On Magn.*, **37,** pp. 2844-2846 (2001).

[6] Mezani S., Atallah K., Howe D., "A high-performance axial-field magnetic gear", *AIP Journal of Applied Physic*, **99**, pp. 08R303-08R303-3 (2006).

[7] Ge Y.-J., Nie C.-Y., Xin Q., "A three dimensional analytical calculation of the air-gap magnetic field and torque of coaxial magnetic gears", *Progress In Electromagnetics Research*, **131**, pp. 391-407 (2012).

[8] Jian L., Deng Z., Shi Y., Wei J., and Chan C. C., "The Mechanism How Coaxial Magnetic Gear Transmits Magnetic Torques Between Its Two Rotors: Detailed Analysis of Torque Distribution on Modulating Ring", *IEEE/ASME Transactions on Mechatronics*, **24**(2), pp. 763-773 (2019).

[9] Jian L., Chau K.T., "A Coaxial Magnetic Gear With Halbach Permanent-Magnet Arrays", *IEEE Trans. on Energy Conv.*, **25** pp. 319-328 (2010).

[10] Jian L., Chau K.T., Li W., and Li J., "A novel coaxial magnetic gear using bulk HTS for industrial applications", *IEEE Trans. On Applied Superconductivity*, **20**, pp. 981-984 (2010).

[11] Jing L., Liu L., Xiong M., and Feng D., "Parameters Analysis and Optimization Design for a Concentric Magnetic Gear Based on Sinusoidal Magnetizations", *IEEE Trans. on Applied Supercon.*, **24**(5), pp. 1-5 (2014).

[12] Kim S.J., Kim C.H., Jung S.Y., Kim Y.J., "Optimal Design of Novel Pole Piece for Power Density Improvement of Magnetic Gear Using Polynomial Regression Analysis", *IEEE Trans. on Energy Conv.*, **30**(3), pp. 1171-1179 (2015).
[13] Afsari S.A., Heydari H., and Dianati B., "Cogging Torque Mitigation in Axial Flux Magnetic Gear System Based on Skew Effects Using an Improved Quasi 3-D Analytical Method", *IEEE Trans. on Magn.*, **51**, pp. 1-11 (2015).
[14] Jungmayr G., Loeffler J., Winter B., Jeske F., and Amrhein W., "Magnetic Gear: Radial Force Cogging Torque Skewing and Optimization", *IEEE Transactions on Industry Applications*, **52(**5), pp. 3822-3830 (2016).
[15] Gardner M. C., Jack B. E., Johnson M., and Toliyat H. A., "Comparison of Surface Mounted Permanent Magnet Coaxial Radial Flux Magnetic Gears Independently Optimized for Volume, Cost, and Mass", *IEEE Transactions on Industry Applications*, **54(**3), pp. 2237-2245 (2018).
[16] Johnson M., Gardner M. C., and Toliyat H. A., "Design Comparison of NdFeB and Ferrite Radial Flux Surface Permanent Magnet Coaxial Magnetic Gears", *IEEE Transactions on Industry Applications*, **54**(2), pp. 1254-1263 (2018).
[17] Wang Y., Filippini M., Bianchi N., and Alotto P., "A Review on Magnetic Gears: Topologies, Computational Models, and Design Aspects", *IEEE Transactions on Industry Applications*, **55**(5), pp. 4557-4566 (2019).
[18] Rahimi M.A., Durali M., and Asghari M., "A Design Approach for Coaxial Magnetic Gear and Determination of Torque Capability", *Journal of Scientia Iranica B*, **25(**2), pp. 772-789 (2018).
[19] Jing L., Zhang T., Gao Y., Qu R., Huang Y., and Ben T., "A Novel HTS Modulated Coaxial Magnetic Gear With Eccentric Structure and Halbach Arrays", *IEEE Transactions on Applied Superconductivity*, **29**(5), pp. 1-5 (2019).
[20] Afsari Kashani S. A., "Rotor Pole Design of Radial Flux Magnetic Gear for Reduction of Flux Density Harmonics and Cogging Torque", *IEEE Transactions on Applied Superconductivity*, **29**(8), pp. 1-8 (2019).
[21] Zhan Y., Ma L., Wang K., Zhao H., Xu G., and Ding N., "Torque Analysis of Concentric Magnetic Gear With Interconnected Flux Modulators", *IEEE Transactions on Magnetics*, **55**(6), pp. 1-4 (2019).
[22] Bahrami Kouhshahi M., Acharya V. M., Calvin M., Bird J. Z., and Williams W., "Designing and experimentally testing a flux-focusing axial flux magnetic gear for an ocean generator application", *IET Electric Power Applications*, **13**(8), pp. 1212-1218 (2019).
[23] Li K., and Bird J. Z., "A Review of the Volumetric Torque Density of Rotary Magnetic Gear Designs", *XIII International Conference on Electrical Machines (ICEM)*, Alexandroupoli, pp. 2016-2022 (2018).
[24] Dianati B., Heydari H., and Afsari S.A., "Analytical Computation of Air-Gap Magnetic Field in a Viable Superconductive Magnetic Gear", *IEEE Trans. on Applied Superconductivity*, **26**, pp. 1-12 (2016).
[25] Liu C., Zhu H., Dong R., Zhou S., and Huang L., "Sensitivity Analysis and Optimal Design of a Linear Magnetic Gear for Direct-Drive Wave Energy Conversion", *IEEE Access*, **7**, pp. 73983-73992 (2019).
[26] Bomela W., Bird J. Z., and Acharya V. M., "The Performance of a Transverse Flux Magnetic Gear", *IEEE Transactions on Magnetics*, **50**(1), pp. 1-4 (2014).
[27] Afsari S.A., Heydari H., and Bashar E., "Viable arcuate double-sided magnetic gear for competitive torque density transmission capability", *Journal of Scientia Iranica D*, **23**(3), pp. 1251-1260 (2016).
[28] Lubin T., Mezani S., and Rezzoug A., "Development of a 2-D analytical model for the electromagnetic computation of axial-field magnetic gears", *IEEE Trans. On Magn.*, **49**, pp. 5507-5521 (2013).
[29] Khatab M. F. H., Zhu Z. Q., Li H. Y., and Liu Y., "Comparative study of novel axial flux magnetically geared and conventional axial flux permanent magnet machines", *CES Transactions on Electrical Machines and Systems*, **2**(4), pp. 392-398 (2018).
[30] Yin X., Pfister P., and Fang Y., "A Novel Magnetic Gear: Toward a Higher Torque Density", *IEEE Transactions on Magnetics*, **51**(11), pp. 1-4 (2015).
[31] Gardner M. C., Johnson M., and Toliyat H. A., "Comparison of Surface Permanent Magnet Axial and Radial Flux Coaxial Magnetic Gears", *IEEE Transactions on Energy Conversion*, **33**(4), pp. 2250-2259 (2018).
[32] Fu W.N., and Li L., "Optimal Design of Magnetic Gears with a General Pattern of Permanent Magnet Arrangement", *IEEE Trans. on Applied Supercon.*, **26**(7), pp. 1-5 (2016).
[33] Aiso K., Akatsu K., and Aoyama Y., "A Novel Reluctance Magnetic Gear for High-Speed Motor", *IEEE Transactions on Industry Applications*, **55**(3), pp. 2690-2699 (2019).
[34] Yin X., Fang Y., and Pfister P., "A Novel Single-PM-Array Magnetic Gear With HTS Bulks", *IEEE Transactions on Applied Superconductivity*, **27**(4), pp. 1-5 (2017).
[35] Li X., Cheng M., and Wang Y., "Analysis, design and experimental verification of a coaxial magnetic gear using stationary permanent-magnet ring", *IET Electric Power Applications*, **12**(2), pp. 231-238 (2018).

LIST OF CAPTIONS

Fig. 1. Exploded view of (a) conventional AMG (b) RAMG.
Fig. 2. Geometric dimensions of RAMG
Fig. 3. Optimization parameters in different layers of RAMG
Fig. 4. Flux lines path in RAMG
Fig. 5. Axial flux density distribution in high and low speed air gaps of optimal RAMG
Fig. 6. Flux density magnitude distribution in different rotors of optimal RAMG (a) stationary PM rotor (b) low speed modulator rotor (c) high speed reluctance rotor
Fig. 7. Static torque of high and low speed rotor in optimal RAMG
Fig. 8. Dynamic torque of high and low speed rotor in optimal RAMG
Table 1. Optimal design parameters of RAMG
Table 2. Output performances of optimal RAMG and initial RAMG

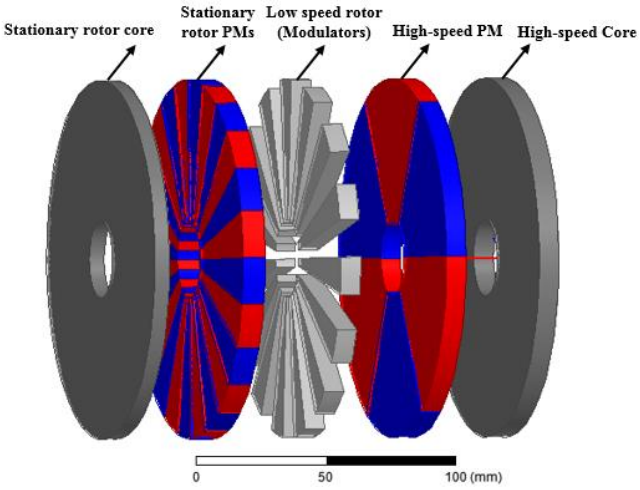

(a)

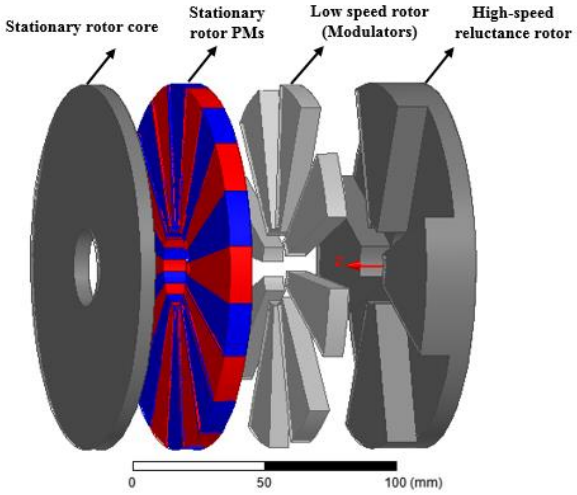

(b)

Fig. 2. Exploded view of (a) conventional AMG (b) RAMG.

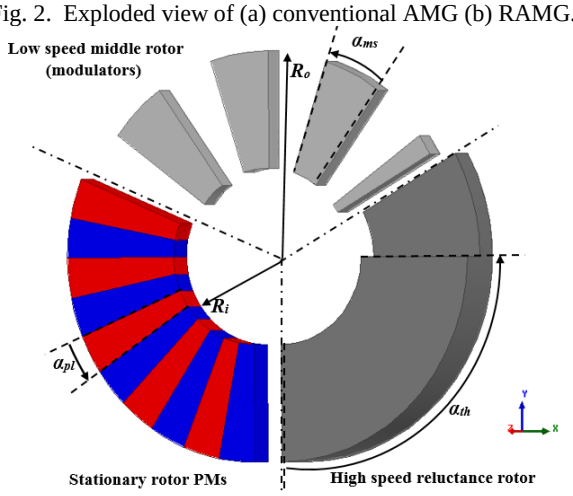

Fig. 2. Geometric dimensions of RAMG

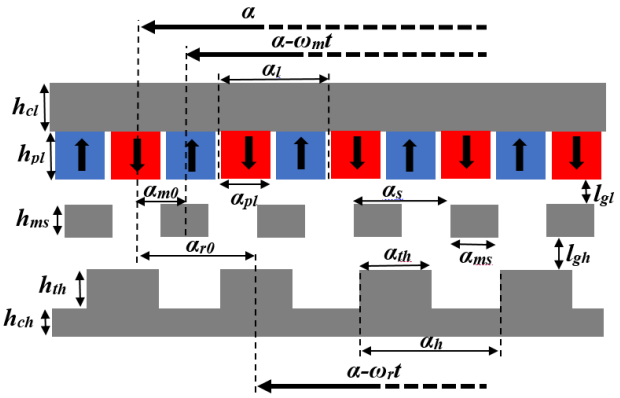

Fig. 3. Optimization parameters in different layers of RAMG

Table 1. Optimal design parameters of RAMG

Design Parameter	Material	variable	Initial Value	Optimal value
Number of high speed rotor teeth	-	n_r	*4*	*4*
Number of stationary rotor pole pairs	-	n_m	*8*	*8*
Number of low speed modulators	-	p_s	*20*	*20*
Air gap length	-	l_{gl},l_{gh}	*1mm*	*1mm*
Outer radius	-	R_o	*70mm*	*70mm*
Inner radius	-	R_i	*15mm*	*15mm*
Axial length of PMs	*NdFeB-35*	$2mm \le h_{pl} \le 10mm$	*4mm*	***9 mm***
Axial length of stationary core	*NGO-M400-50A5*	$3mm \le h_{cl} \le 8mm$	*4mm*	***6 mm***
Axial length of modulators	*NGO-M400-50A5*	$2m \le h_{ms} \le 10mm$	*5mm*	***8 mm***
Axial length of reluctance teeth	*NGO-M400-50A5*	$2mm \le h_{th} \le 15mm$	*5mm*	***11 mm***
Axial length of high speed core	*NGO-M400-50A5*	$5mm \le h_{ch} \le 10mm$	*5mm*	***8 mm***
Pole arc to pole pitch ratio of PMs	-	$0.25 \le \alpha_{pl}/\alpha_l \le 0.5$	*0.4*	***0.5***
Teeth arc to teeth pitch ratio	-	$0.25 \le \alpha_{th}/\alpha_h \le 0.5$	*0.3*	***0.5***
Slot opening of modulators	-	$0.25 \le \alpha_{ms}/\alpha_s \le 0.5$	*0.5*	***0.5***
Remanence of PMs	-	B_r	*1.2T*	*1.2T*

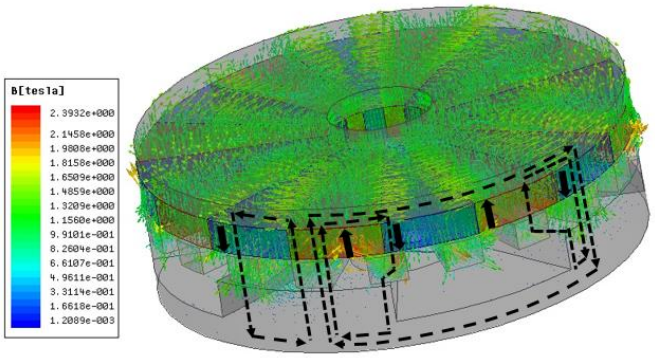

Fig. 4. Flux lines path in RAMG

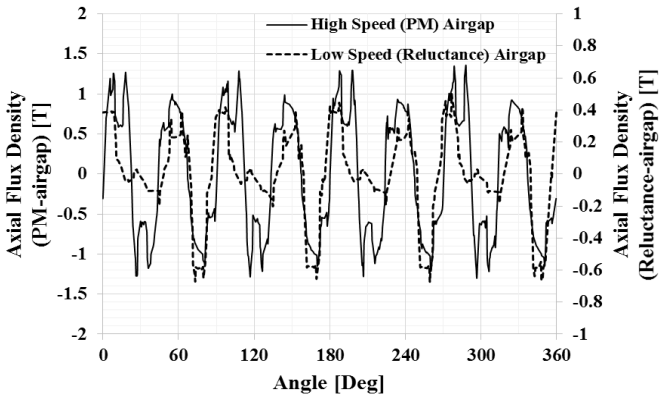

Fig. 5. Axial flux density distribution in high and low speed air gaps of optimal RAMG

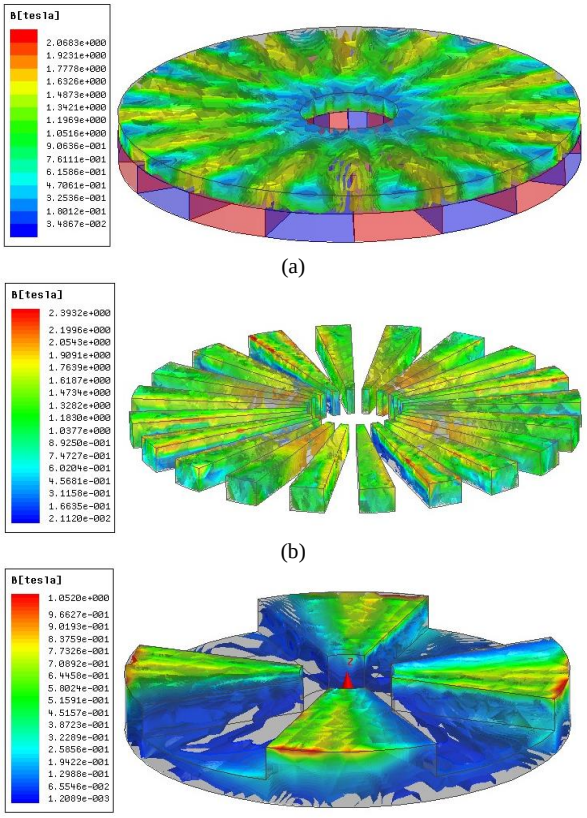

Fig. 6. Flux density magnitude distribution in different rotors of optimal RAMG (a) stationary PM rotor (b) low speed modulator rotor (c) high speed reluctance rotor

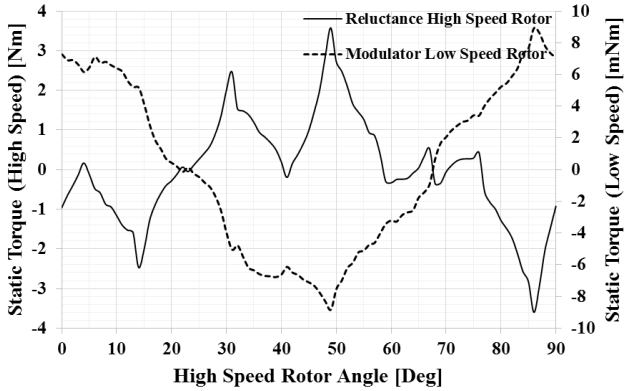

Fig. 7. Static torque of high and low speed rotor in optimal RAMG

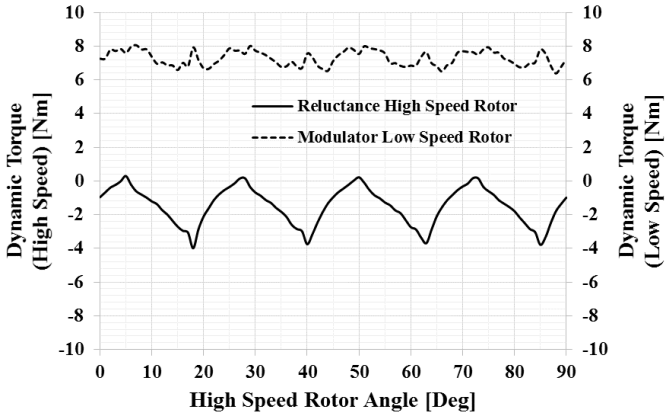

Fig. 8. Dynamic torque of high and low speed rotor in optimal RAMG

Table 2. Output performances of optimal RAMG and initial RAMG

Output Parameter	Initial RAMG	Optimal RAMG
High speed static Torque	*0.74 Nm*	*1.5 Nm*
Low speed static Torque	*3.73 Nm*	*7.5 Nm*
Dynamic cogging torque (high speed)	*3.08Nm*	*4.3 Nm*
Dynamic cogging torque (low speed)	*1.03 Nm*	*1.7 Nm*
Torque Density	*9.6 kNm/m^3*	*11.07 kNm/m^3*

BIOGRAPHY

Seyed Ahmadreza Afsari received B.S. degree in electrical engineering from K.N.Toosi University of Technology, Tehran, Iran, in 2007 and the M.Sc. degree from the University of Kashan, Kashan, Iran, in 2010, both in electrical power engineering and the Ph.D. degree from the Iran University of Science and Technology, Tehran, Iran in 2016. Following graduation, he joined University of Kashan, Kashan, Iran, as an Academic Member (Assistant Professor) of the Electrical Power Group. His research interests are magnetic gears, analytical methods, finite-element-method-based simulation techniques, optimization methods, and applied superconductors in power systems.